

Article

Global Mapping of GDP at 1 km² Using VIIRS Nighttime Satellite Imagery

Xuantong Wang ^{1,*}, Paul C. Sutton ¹ and Bingxin Qi ²

¹ Department of Geography and the Environment, University of Denver, Denver, CO 80208, USA; paul.sutton@du.edu

² Morgridge College of Education, University of Denver, Denver, CO 80210, USA; bingxin.qi@du.edu

* Correspondence: Xuantong.wang@du.edu; Tel.: +1-510-599-8566

Received: 5 November 2019; Accepted: 7 December 2019; Published: 11 December 2019



Abstract: Frequent and rapid spatially explicit assessment of socioeconomic development is critical for achieving the Sustainable Development Goals (SDGs) at both national and global levels. Over the past decades, scientists have proposed many methods for estimating human activity on the Earth's surface at various spatiotemporal scales using Defense Meteorological Satellite Program Operational Line System (DMSP-OLS) nighttime light (NTL) data. However, the DMSP-OLS NTL data and the associated processing methods have limited their reliability and applicability for systematic measuring and mapping of socioeconomic development. This study utilized Visible Infrared Imaging Radiometer Suite (VIIRS) NTL and the Isolation Forest machine learning algorithm for more intelligent data processing to capture human activities. We used machine learning and NTL data to map gross domestic product (GDP) at 1 km². We then used these data products to derive inequality indexes (e.g., Gini coefficients) at nationally aggregate levels. This flexible approach processes the data in an unsupervised manner at various spatial scales. Our assessments show that this method produces accurate subnational GDP data products for mapping and monitoring human development uniformly across the globe.

Keywords: nighttime light; VIIRS; GDP; sustainability; machine learning

1. Introduction

The United Nations has established a set of sustainable development goals to achieve a better future for people and the planet. Building on the success of the Millennium Development Goals (MDGs), the 2030 Agenda for Sustainable Development aims to promote and stimulate a series of actions to transform our world. The 17 Sustainable Development Goals (SDGs) with 169 associated targets will unite and mobilize efforts from countries across the world to tackle and address urgent development issues like poverty, inequality, and climate change [1–4]. Although significant progress has been made towards the achievement of these goals, some of the actions and policies have not been implemented effectively because of the complexity of the Earth system and human–environment interactions. In other words, global climate change is progressing at a quick pace and many people are still living in poverty. Therefore, it is important to understand the global distribution of wealth, characterize socioeconomic well-being, and predict environmental change at appropriate spatiotemporal resolutions to facilitate the implementation of policies and the achievement of SDGs [5].

Measuring socioeconomic data in a timely and accurate manner is important for evaluating current socioeconomic status and assessing policy effectiveness. Doing this well helps countries achieve many of the SDGs including sustainable development, eradication of poverty, and reduction of inequality and exclusion. It also helps practitioners, scientists, and policymakers compare levels of development across the globe to inform efforts toward achieving the SDGs. However, collecting these data can be

costly and challenging for many less-developed countries. In recent years, the availability of remotely sensed images has greatly helped scientists monitor human activity on the Earth [6]. For instance, nighttime light (NTL) data are widely used for estimating and evaluating socioeconomic activities since they can capture the artificial light on the Earth's surface [7–9]. Remote sensing technology and satellite imagery have provided us with global and regional economic data to understand and evaluate the relationship between human development and nature [10]. There are many difficulties associated with collecting traditional census data for measuring human well-being. For example, accurate information about the size and distribution of the human population is not available for many regions of the world and sometimes these data are of poor quality [11]. Hence, remote sensing data can be an alternative way for scientists to study and monitor human activities in a timely, consistent, and affordable way. NTL data are different from other remote sensing data as they capture the artificial light on the Earth's surface and offer a unique view of human activity [9,12–16]. For example, NTL imagery has been used to generate and demonstrate the quantitative relationships between the NTL and population and energy consumption in the USA [17,18].

The Visible Infrared Imaging Radiometer Suite (VIIRS) platform is a new and improved vehicle for developing global NTL data products. Prior to VIIRS, the Defense Meteorological Satellite Program Operational Line System (DMSP-OLS) was primarily designed and developed for cloud cover image detection. Researchers discovered that DMSP-OLS nighttime images of the visible and near-infrared (VNIR) band could help scientists observe and detect the VNIR emission sources (e.g., city lights, auroras, gas flares, and fires). Thus, the DMSP-OLS NTL data have been used in many fields including (1) the measuring of human settlements, (2) urban population and socioeconomic activity, (3) energy and electricity consumption, (4) the monitoring of gas flaring, (5) forest fires, and (6) the impacts of military actions and natural disasters [19]. In recent years, the Visible Infrared Imaging Radiometer Suite (VIIRS) sensor, which is equipped with the Day/Night Band (DNB), has outperformed its predecessor DMSP-OLS in many ways. In general, VIIRS exceeds DMSP-OLS including greater dynamic range, finer spatial resolution, and lower detection limits [20,21].

Over the past decades, scientists have proposed many methods to estimate GDP at national and subnational levels using NTL [19,22–24]. For example, Sutton et al. [25] estimated the marketed and non-marketed economic value on a global scale and discovered that the GDP was correlated with the amount of light energy emitted by that country based on DMSP-OLS NTL. Shi et al. [26] used VIIRS NTL to estimate GDP and electricity power consumption and concluded that it can be a strong tool to evaluate socioeconomic indicators. Nevertheless, some researchers found that using NTL alone is insufficient to capture the spatial heterogeneity of GDP at subnational levels. First of all, NTL is not a direct measurement of socioeconomic activities. In addition to that, in many developing regions like Sub-Saharan Africa, a large portion of the population are engaged in agricultural activities. Thus, using NTL alone cannot estimate GDP accurately in these regions [27]. Therefore, some researchers have started to estimate various socioeconomic indicators using NTL based on urban and rural regions separately in order to capture the different levels of productivity [28].

This paper presents an approach that utilizes the VIIRS NTL data for estimating the socioeconomic development metrics for the world. We mainly studied socioeconomic development with a focus on the measurement of inequality as these indicators can reflect the socioeconomic status and the current level of development. Rising levels of economic inequality can lead to a series of consequences including lower rates of economic growth, happiness, and higher rates of crime, health, and poverty problems [29]. Moreover, to improve the current data processing method to achieve better results, we separated GDP estimation based on rural and urban regions using land cover classification data. In addition to that, we also used a machine learning-based data processing method for filtering the NTL outliers that were not related to socioeconomic activities to capture spatial heterogeneity of GDP distribution at the pixel level. We adopted the unsupervised Isolation Forest (iForest) machine learning model to help us automatically detect and remove irrelevant NTL data so as to improve model accuracy [30]. We applied this method to develop two NTL-based indexes including (1) NTL-Gini,

which is adapted from the Gini coefficient and developed based on the cumulative share of population and gross domestic product (GDP) and (2) NTL-2020, which is adapted from the 20:20 ratio and used to show how much richer the top 20% of populations are to the bottom 20% based on the cumulative distribution of GDP and population. We produced the two NTL-based indexes to investigate and estimate the current development progress for countries around the world [31].

This paper is organized as follows. Section 2 describes the data and methods we used for developing NTL-based indexes and the model that was developed for evaluating social and economic status. In Sections 3 and 4, we present and evaluate the results and compare them with the actual data. Finally, we summarize the results and draw conclusions in Section 5.

2. Materials and Methods

2.1. Data Collections

The datasets used in this study are described in Table 1. This study used multisource geospatial data in tandem with aggregate national socioeconomic data to develop NTL-based inequality indexes. We used the stable, cloud-free VIIRS NTL (vcm-orm-ntl) product which is produced by the National Oceanic Atmospheric Administration (NOAA) and the National Aeronautics and Space Administration (NASA). We selected the “vcm-orm-ntl” data to calculate the sum of total NTL intensity in the urban region for each of the administrative units to estimate the development in the urban regions. The NTL can be used to estimate economic activities contributed by commercial and industrial activities. This product improves our estimates of socioeconomic data, since it contains cloud-free average radiance values and the outliers caused by fires and other ephemeral light have been removed. The administrative boundary file was collected from the Database of Global Administrative Areas (GADM) [32]. We mainly used the country (level 0) and subdivision level (levels 1 and 2) data for national and subnational data processing. Additionally, population distribution and settlement data at the 1 km² level were obtained from the Global Human Settlement (GHS) datasets, which contain location, population, and urban extent information for the human presence on the planet from 1975 to 2015. Human settlement information was obtained from the GHS Settlement Model grid (SMOD), which contains urban center (densely populated areas), urban clusters (towns and suburbs), and rural grid cells (rural areas) that can help us separate urban regions from rural regions. The population data of GHS contain the distribution and density of population and they are expressed as the number of people in each cell. For example, Figure 1 shows the NTL, SMOD, and population data distribution in mainland China and Afghanistan. Socioeconomic statistics were obtained from the World Bank and United Nations Development Programme (UNDP) databases. We used income classification data to group countries and agriculture, forestry, and fishing with value added (% of GDP) for calculating the proportion of GDP in rural regions to estimate the agriculture activity.

Table 1. Table of data inputs for estimating GDP and inequality indexes.

Dataset	Description	Sources
Population	Global spatial information for the human presence on the planet in 2015 with 1 km ² spatial resolution.	GHS [33]
Human Settlement	Global spatial information for the human settlement (urban and rural) in 2015 with 1 km ² spatial resolution.	GHS [34]
VIIRS	VIIRS Cloud Mask-Outlier Removed-Night-Time Lights (vcm-orm-ntl) annual data from 2015 with a spatial resolution of 15 arc-second.	NOAA/NASA [35]
Global Administrative Areas	Global administrative areas of countries including the sub-divisions (v3.6).	GADM [32]
Productivity Ratios	Agriculture, forestry, and fishing with value added (% of GDP) from 2015 at national level.	The World Bank [36]
National GDP	2015 National GDP at purchasing power parity in constant 2011 U.S. dollars.	The World Bank [36]
Gini Index	Gini index estimates based on household survey data from 2015 at national level.	The World Bank [36]
Income Quintile Ratio	Ratio of the average income between the richest 20% and the poorest 20% of the population. Only 2013 income quintile ratios are available.	UNDP [37]

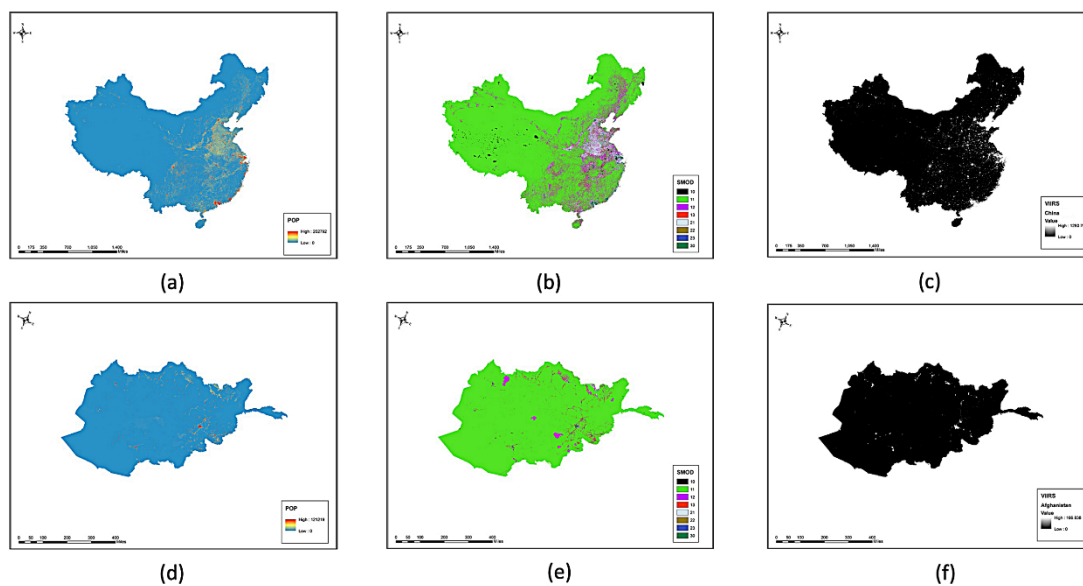


Figure 1. (a) NTL for mainland China, (b) GHS SMOD data for mainland China, (c) GHS population data for mainland China, (d) NTL for Afghanistan, (e) GHS SMOD data for Afghanistan, (f) GHS population data for Afghanistan.

2.2. Data Pre-Processing

Results from previous studies show that using NTL alone is insufficient to accurately measure the GDP at subnational levels [27]. In order to assess the different levels of socioeconomic development in the country, we separated the data into urban and rural data to capture the different levels of industrial, commercial, and agricultural activities on a subnational scale using level 0, 1, and 2 administrative districts from GADM. The data preparation consisted of three steps (Figure 2). In step 1, we converted GHS population raster data to points in ArcGIS Pro 2.4.1 and used the converted population data points to sample and extract the values of human settlement information and NTL intensity values based on SMOD data and VIIRS NTL. Therefore, all data points contained attribute information of population, nighttime light value, SMOD, administrative districts information at different levels, income classification (based on country), and unique point identifier. In step 2, we separated population data into urban and rural data based on the SMOD value. In step 3, we applied the iForest method to identify NTL outliers in urban regions that were not related to socioeconomic activities and reclassified them as 0.

Although we selected the “vcm-orm-ntl”, irrelevant light sources that are not filtered by the product processing algorithm still remain due to its sensitivity [28]. Moreover, NTL is not directly measuring socioeconomic activities and contains irrelevant data that can greatly affect the GDP estimates especially at the 1 km² level [38,39]. Therefore, we adopted a series of measures to remove these irrelevant data in step 3. Since we were only using NTL to measure GDP in the urban regions, we first filtered the data by selecting the data points in the urban regions based on their attributes (SMOD value >20). Then, we used the unsupervised machine learning model of iForest to detect the anomalies for the urban pixels based on the population and NTL attributes of urban data points. Over the past decades, many anomaly detection models have been developed based on classification, clustering, and statistical methods. Some researchers have used the DMSP data as a mask to extract the VIIRS data or build a normal profile for the NTL data in order to remove outliers based on the range of NTL intensity value distribution. However, it is very difficult to apply this method globally due to the variations among countries. Furthermore, some of the methods can only be applied to data of low dimensionality and smaller size. By contrast, the iForest machine learning model can automatically detect irrelevant NTL outliers [30] because it is (1) not reliant on the distribution profile of NTL data, (2) more suitable for processing large datasets, and (3) specifically designed to detect

anomalies. Studies have demonstrated that the iForest method can outperform many other existing model-based, distance-based, and density-based methods [30]. It is also more suitable for processing large datasets compared to traditional methods like the density-based spatial clustering of applications with noise (DBSCAN) [40]. We used data points for all countries as input so that iForest could detect outliers based on the population and NTL values' patterns. For instance, points with extremely high NTL value and low population were identified as anomalies (Figure 3). The identified NTL outlier values were changed to 0. Since we had already used a filtered VIIRS NTL product, only a small proportion (about 0.1%) of NTL outliers were detected.

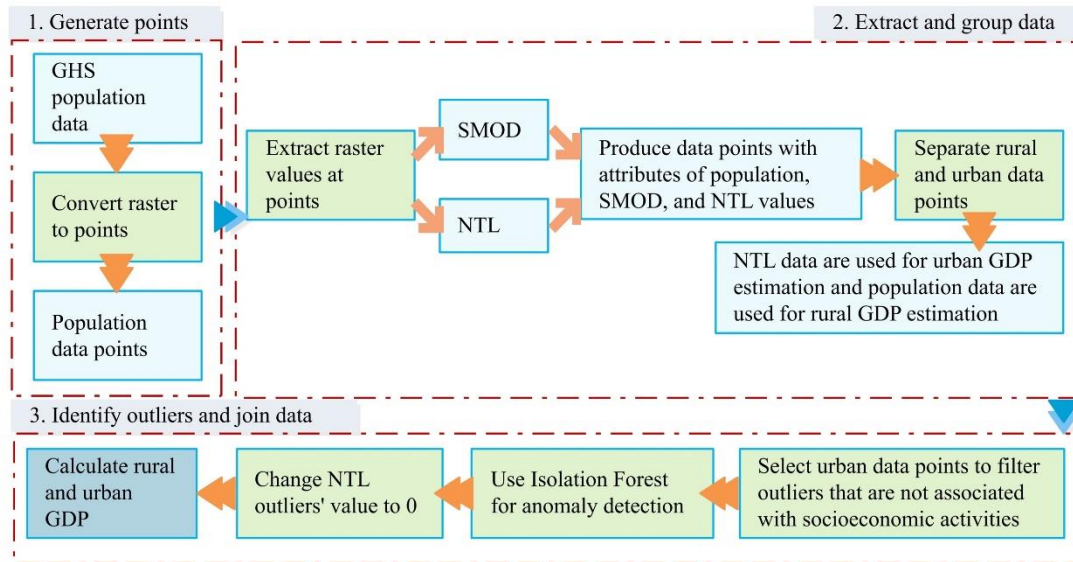


Figure 2. Procedures for processing population, SMOD, and NTL data.

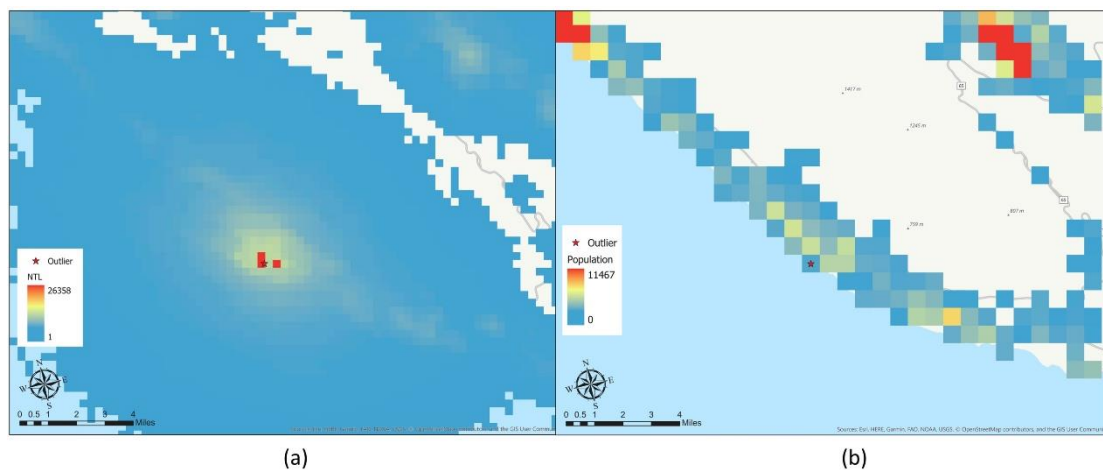


Figure 3. Sample result from iForest outlier detection. Outlier identified in Iran that there is (a) very high NTL value and (b) low population density in the coastal region.

2.3. GDP and Inequality

The Gini coefficient is a statistical measure of economic inequality based on income distribution [41,42]. A higher Gini coefficient value indicates a higher degree of income inequality, whereas a lower value indicates a lower degree of income inequality. Elvidge et al. [12] developed the night light development index (NLDI) based on the Lorenz curve analysis to analyze the co-distribution of NTL and population by sorting the NTL values in an ascending order. Nevertheless, this index may not be sufficient to capture the distribution of economic activity as it cannot accurately represent the

spatiotemporal variation of income distribution since NTL is not a direct measure of income or wealth. Therefore, we combined the NTL values (nanoWatts/cm²/sr) with the actual agricultural production ratios and population distribution in order to improve this characterization of economic activity. We used (1) the urban data points (SMOD value >20) with NTL values to measure the distribution of economic activity in the urban regions and (2) the rural data points (SMOD value <20) with population density to measure the distribution of economic activities in the rural regions. We obtained the aggregate GDP in each district based on the sum of rural and urban GDP (in constant 2011 U.S. dollars) for that district. We defined the urban (UV_i) and rural pixel value (RV_i) of GDP as follows:

$$UV_i = \frac{SnNTL * (1 - AgRatio) * GDP * PopV_i}{TotNTL * TotUrPop} \quad (1)$$

$$RV_i = \frac{PopV_i * AgRatio * GDP}{TotRuPop} \quad (2)$$

where *i* is the unique identification of population pixel (derived from the GHS population layer), SnNTL is the total NTL in the district, TotNTL is the total NTL for the country, PopVi is the population count of the corresponding pixel, TotRuPop and TotUrPop are the total rural and urban population for the country, AgRatio is the proportion of agriculture production of the total GDP, and GDP is the national GDP at purchasing power parity (in 2011 constant U.S. dollars) data obtained from the World Bank database. Based on the procedures described above, we produced a gridded GDP product at the 1 km² level for countries around the world (Figure 4). The subnational GDP calculation was based on the aggregate NTL and population using level 2 GADM districts. In addition, for countries without AgRatio data, we used the total rural population divided by the total national population to calculate the estimated AgRatio.



Figure 4. Gridded GDP product at 1 km² level.

NTL-Gini and NTL-2020 ratios were calculated based on the accumulative distribution of aggregate GDP at level 1 and 2 districts for countries around the world. We sorted the aggregate GDP data at district level in an ascending order to construct a GDP distribution profile for each country based on the fraction of population and the cumulative share of GDP at the subnational levels and to plot the

Lorenz curve (Figure 5). The NTL-Gini coefficient is equal to the area marked A divided by the sum of the areas marked A and B in Figure 5a (Gini index = Area A/(Area A + Area B)).

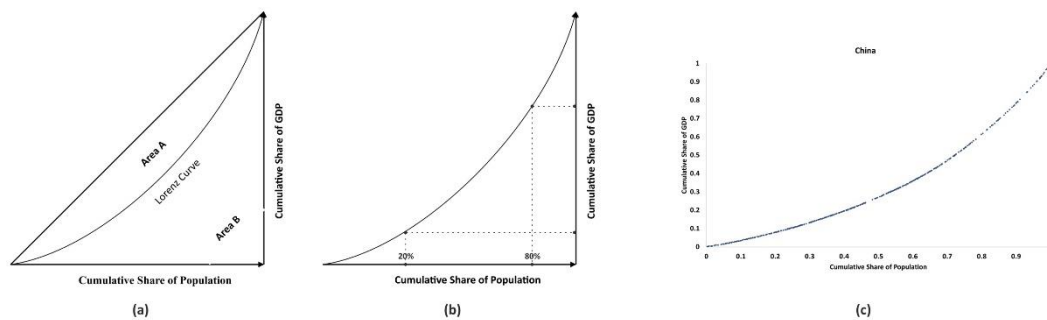


Figure 5. Lorenz curve for Gini and 20:20 ratios estimation. Calculation of (a) NTL-Gini and (b) NTL-2020 ratios based on the Lorenz curve, and (c) sample Lorenz curve for China based on the cumulative distribution of population and GDP.

Moreover, we also calculated the 20:20 ratio based on the distribution of NTL GDP at district level to measure inequality (Appendix A). Higher 20:20 ratios indicated higher income inequality [43–45]. The 20:20 ratio can be more revealing than the Gini coefficient since it compares how much wealthier the top 20% of the population is to the bottom 20% of the population. Many studies have shown that this can be a more useful measure to evaluate other development issues like health and social problems. In order to calculate the 20:20 ratio, we used the same distribution profile for each country and calculated the ratio between the total GDP for the top 20% of the population and total GDP for the bottom 20% of the population.

3. Results

3.1. Subnational GDP Validation

The performance of NTL-based development indexes was evaluated using the actual GDP data from the Organisation for Economic Co-operation and Development (OECD) Regional Statistics and Indicators, the Gini coefficient data from the World Bank databank, and the 20:20 Ratios from UNDP. We first compared and validated the subnational GDP products by using the 249 regional GDP (Large regions TL2) data from OECD administrative units that matched the level 1 districts from GADM. Regional total GDP results of the NTL-based GDP were aggregated using the zonal statistics tool in ArcGIS Pro based on the 1 km² gridded NTL GDP product. We produced the cross-sectional fit comparing the NTL-based GDP against the actual GDP from OECD regions. In Figure 6, the overall result shows that NTL-based subnational GDP has a high coefficient of determination ($R^2 = 0.761$). In addition, since many researchers have studied the relationship between total NTL values within regions with GDP [26,46] based on simple linear regression, we also produced the cross-sectional fit comparing the sum of NTL within districts against the actual GDP from OECD regions ($R^2 = 0.684$). Results in Figure 6 show that NTL GDP can better reflect the actual GDP values. Nevertheless, due to the small size of validation data ($n = 246$), it is difficult for us to evaluate the results' accuracy globally at various spatial scales.

We also compared our data based on the electricity accessibility [47] and the Gridded GDP datasets [48]. Figure 7 shows that because the Gridded GDP datasets only contain GDP per capita information for Uganda at the national level, the GDP data (Figure 7c) is mainly dependent on population density (Figure 7a). Therefore, it fails to show the subnational variation of economic activities in urban and rural regions. Figure 7b shows the electricity access estimation (distribution of people without access to electricity) near Kampala, Uganda [47]. Both the NTL GDP data and the electricity access rate show that the Gridded GDP dataset [48] overestimates GDP in many regions outside Kampala despite the fact that these regions have a low electricity access rate and are less

developed. This is possibly because the Gridded GDP product is incapable of differentiating levels of productivity within districts and fails to capture the spatial heterogeneity of GDP at various spatial scales.

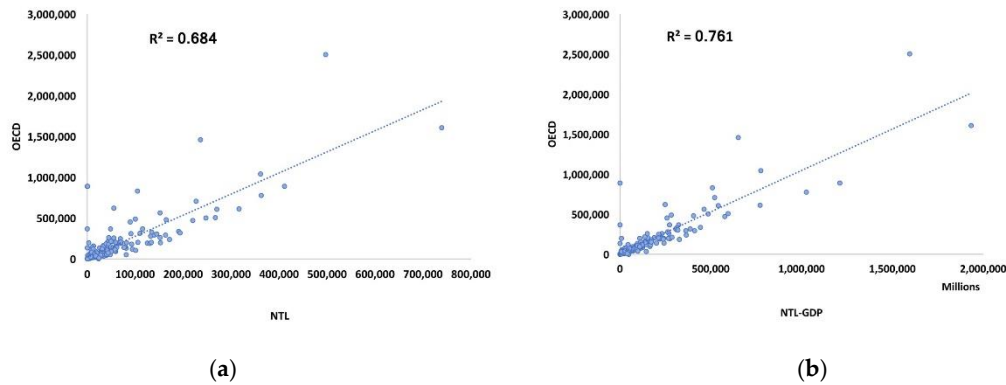


Figure 6. (a) Scatterplot of Organisation for Economic Co-operation and Development (OECD) regional GDP and sum of NTL values within districts, and (b) scatterplot of OECD regional GDP and district-level NTL GDP ($n = 246$ subnational districts).

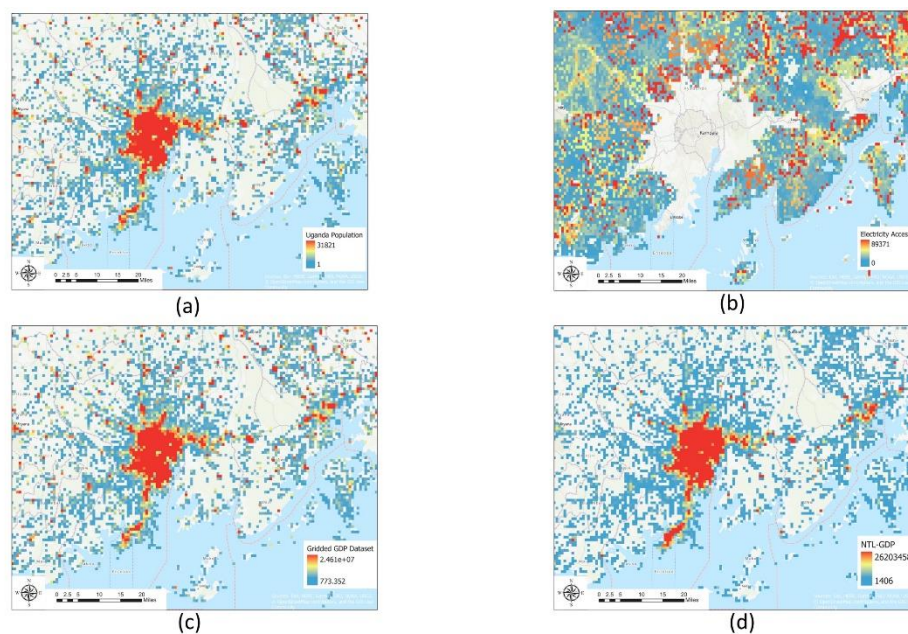


Figure 7. Comparisons of population distribution, electricity accessibility [47], Gridded GDP at the 1 km^2 level [48], and NTL GDP data around Kampala, Uganda. (a) Population data, (b) electricity access data, (c) GDP data from Gridded global datasets, (d) NTL-based GDP.

3.2. Inequality Validation

To evaluate whether NTL-based GDP distribution can predict inequality accurately, we compared the NTL-based inequality indexes against the actual Gini index and 20:20 ratios data using root mean square error (RMSE) and mean absolute error (MAE) (Figure 8). We normalized all inequality data into the range of 0 to 1. We also compared the data by categorizing the countries based on the income level classification. The overall RMSE and MAE for all countries without using income classification were also compared. The inequality validation results show that there is an overall smaller deviation between the NTL-2020 ratios and the actual data from UNDP, indicating that using NTL and population data can better capture the differences of wealth distribution for the top and bottom 20% of the population in urban and rural regions. Both of the NTL-based Gini coefficient and NTL-2020 have similar RMSE

and MAE for high-income and low-income countries, whereas the NTL-2020 ratios have smaller RMSE and MAE for upper-middle and lower-middle countries. This shows that the overall GDP distribution profile may be more accurate for developed and less-developed countries as they tend to rely more on tertiary industry (that can be captured by NTL) and primary industry (captured by population density). For many developing countries (with upper-middle and lower middle incomes), where there tends to be greater socioeconomic inequality, the NTL-2020 ratios can better capture this unequal distribution of income and opportunity. For instance, studies [27] have shown that the correlation between light intensity values and economic activity is much weaker for countries that are dependent on agriculture. This is probable since most of these countries are developed countries or industrialized countries that have advanced their technology infrastructures and developed their economies. Therefore, it is harder to measure the socioeconomic development in these countries.

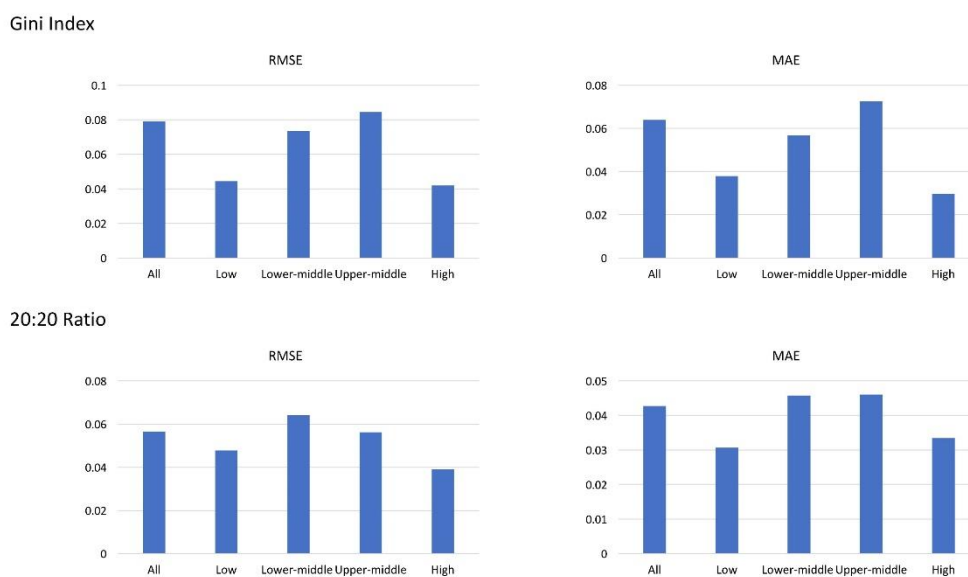


Figure 8. Validation of NTL-based Gini coefficient and 20:20 ratios based on root mean square error (RMSE) and mean absolute error (MAE) for all countries, low-income countries, lower-middle income countries, upper-middle income countries, and high-income countries.

4. Discussion

The NTL global GDP data at 1 km² can be aggregated into different subnational levels to support analysis at multiple spatial scales. In general, the NTL data collected by the VIIRS can help us not only monitor the light sources but also study various human activities. By using the multisource data, we developed an NTL-based index to estimate different levels of socioeconomic development in urban and rural regions in an efficient and accurate manner. The VIIRS data were capable of capturing commercial and industrial activities more accurately than DMSP-OLS. Although DMSP-OLS NTL data have been widely used due to their detection of anthropogenic lighting sources to study human activities, they still present many significant problems. For instance, the data have deficiencies such as coarse spatial resolution, saturation, lack of in-flight calibration, and lack of low-light imaging spectral bands suitable for discriminating lighting types [8]. Elvidge et al. [20] compared capabilities of DMSP-OLS and VIIRS and concluded that VIIRS is superior to DMSP-OLS in many ways. Therefore, as more VIIRS products are released (monthly and annual), there is a great potential to capture human development at various spatiotemporal scales. Furthermore, the NTL imagery can potentially become an alternative method for scientists to measure and assess socioeconomic development to achieve SDGs. First, there are many limitations for collecting and calculating traditional inequality data. NTL can help us generate reliable estimates to evaluate if cities have achieved the sustainable goals on a global scale. Second, NTL estimates can be combined with multisource data to help people understand

the current water, energy, and food security nexus to evaluate and manage the capacity of our growth. Third, it is important to develop different measures based on various sources of data and evaluate the nation's sustainable development based on multiple indexes. The current method is also limited by the availability of accurate data for model optimization and validation. For example, in our model, we assumed that the rural region was mainly dependent on agricultural activities. However, there are also other labor-intensive activities that can contribute to the rural GDP like mining, oil extraction, and refinery. Therefore, it is also important to collect more accurate socioeconomic data on various spatial scales to improve the accuracy of GDP estimates.

5. Conclusions

Our approach is suitable for measuring the distribution of GDP on both subnational and national levels. The NTL-based GDP estimation using urban and rural separation helped us capture the spatial heterogeneity of GDP distribution compared to the simple linear regression method based on NTL values only. By utilizing the iForest machine learning solution, it was easier for us to detect outliers from the urban NTL data to better estimate GDP distribution at the pixel level (1 km²). Furthermore, the NTL-based indexes were useful for estimating a variety of inequality indicators. Nevertheless, due to the different levels of development, the performance of NTL-based indexes was also affected. In the future, several options can take this research to another level: (a) incorporating an advanced machine learning model or hybrid model to improve the model performance; (b) collecting more historical socioeconomic data to analyze development changes based on the trend and make forecasts for the future; (c) estimating the inequality at subnational levels and validating the results using ground-truth data; and (d) incorporating more variables to train the model so that it can be customized and adjusted for different inequality evaluation purposes. Moreover, monthly VIIRS NTL products are now also available. There is a great potential for us to understand the dynamics of human population changes within cities, assess our ecological footprints, estimate the demand of resources, and evaluate the limit of our growth [49–51].

Author Contributions: Conceptualization, Paul C. Sutton and Xuantong Wang; methodology, all of the authors; validation, all of the authors.

Funding: This research received no external funding.

Acknowledgments: This work was supported in part by the Microsoft AI for Earth grant.

Conflicts of Interest: The authors declare no conflict of interest.

Appendix A

Table A1. NTL-Gini and NTL-2020 results.

Country	NTL-Gini	NTL-2020
American Samoa	0.010	1.057
Solomon Islands	0.018	1.100
San Marino	0.035	1.161
Cyprus	0.039	1.202
New Caledonia	0.053	1.291
Belize	0.054	1.353
Guam	0.078	1.498
Bermuda	0.079	1.409
Tonga	0.082	1.789
Qatar	0.103	1.580

Table A1. Cont.

Country	NTL-Gini	NTL-2020
Spain	0.109	1.747
Cayman Islands	0.120	2.619
Virgin Islands (U.S.)	0.121	1.788
Libya	0.123	1.854
Trinidad and Tobago	0.123	1.901
Italy	0.131	2.010
Greece	0.137	1.844
Israel	0.141	1.994
Liechtenstein	0.149	2.013
Belgium	0.152	2.268
Saudi Arabia	0.156	2.141
Singapore	0.158	2.099
Bosnia and Herzegovina	0.167	2.466
Finland	0.167	2.420
Iceland	0.168	4.659
Malta	0.168	2.175
Chile	0.171	2.431
Bahamas, The	0.173	2.877
Kuwait	0.181	2.563
Albania	0.189	2.698
Bahrain	0.190	2.540
Barbados	0.190	4.441
Uruguay	0.197	2.965
Argentina	0.198	2.878
St. Vincent and the Grenadines	0.202	3.381
Kyrgyz Republic	0.202	3.158
Jamaica	0.204	2.934
France	0.206	3.050
Hong Kong SAR, China	0.212	2.718
Sierra Leone	0.214	2.793
Nepal	0.215	2.863
Jordan	0.216	2.728
Japan	0.220	3.224
Korea, Rep.	0.222	3.103
Dominican Republic	0.223	3.647
United Kingdom	0.224	3.161
Latvia	0.226	3.747
Armenia	0.227	2.915
Puerto Rico	0.228	3.541
New Zealand	0.233	4.454

Table A1. Cont.

Country	NTL-Gini	NTL-2020
Morocco	0.235	3.296
Serbia	0.239	4.004
Malaysia	0.245	3.873
Turkmenistan	0.254	3.671
Togo	0.254	3.840
Mongolia	0.256	4.181
Montenegro	0.259	5.175
Iran, Islamic Rep.	0.259	3.299
Czech Republic	0.262	3.669
Egypt, Arab Rep.	0.262	3.541
Canada	0.263	4.361
Bangladesh	0.265	4.117
Switzerland	0.266	4.482
Belarus	0.268	4.785
Ireland	0.269	4.082
Brazil	0.276	5.263
Germany	0.277	4.293
Australia	0.279	4.875
Peru	0.279	6.108
Pakistan	0.280	4.334
Lebanon	0.280	3.699
Tajikistan	0.282	4.011
Ecuador	0.288	5.204
Portugal	0.289	9.392
Hungary	0.291	5.646
Tunisia	0.294	4.615
Turkey	0.296	4.884
United States	0.297	6.125
Andorra	0.299	113.727
Costa Rica	0.299	5.939
Algeria	0.301	4.461
Antigua and Barbuda	0.302	35.927
Luxembourg	0.304	18.170
Bolivia	0.307	6.176
North Macedonia	0.308	4.890
Comoros	0.311	7.412
South Africa	0.311	6.693
Colombia	0.311	7.124
Côte d'Ivoire	0.312	4.120
China	0.314	4.654

Table A1. Cont.

Country	NTL-Gini	NTL-2020
Uzbekistan	0.314	5.460
Oman	0.316	4.982
Venezuela, RB	0.316	4.780
West Bank and Gaza	0.317	6.818
Mexico	0.317	6.849
Mauritius	0.318	5.428
United Arab Emirates	0.319	5.260
Cuba	0.320	5.631
Sweden	0.320	7.993
Mali	0.321	5.199
Guyana	0.322	5.355
Paraguay	0.324	5.810
Indonesia	0.326	5.033
Guinea-Bissau	0.326	5.975
Bulgaria	0.332	14.342
Georgia	0.335	7.281
Lesotho	0.336	7.861
Liberia	0.336	4.940
Austria	0.337	7.776
Poland	0.343	6.219
Isle of Man	0.345	94.870
Panama	0.353	17.050
Dominica	0.356	5.079
Lithuania	0.362	11.281
Honduras	0.366	7.189
Iraq	0.367	9.034
Suriname	0.368	8.129
Denmark	0.369	7.777
El Salvador	0.371	7.590
Ghana	0.371	6.551
Slovak Republic	0.374	6.704
Myanmar	0.375	6.744
India	0.381	7.201
Syrian Arab Republic	0.383	9.901
Gambia, The	0.388	7.404
Ukraine	0.399	6.813
Russian Federation	0.399	10.015
Azerbaijan	0.402	8.961
Croatia	0.409	27.197
Vanuatu	0.409	5.782

Table A1. Cont.

Country	NTL-Gini	NTL-2020
St. Lucia	0.411	15.134
Grenada	0.416	7.682
Nicaragua	0.417	14.450
Brunei Darussalam	0.423	19.773
Thailand	0.428	9.299
Burkina Faso	0.428	8.286
Benin	0.429	8.287
Haiti	0.439	10.196
Fiji	0.446	15.726
Ethiopia	0.456	8.087
Congo, Rep.	0.456	33.783
Cameroon	0.457	12.810
Senegal	0.460	11.864
Equatorial Guinea	0.463	33.041
Angola	0.466	21.985
Moldova	0.468	10.032
Djibouti	0.468	81.186
Niger	0.472	9.449
Botswana	0.473	12.043
Rwanda	0.477	9.348
Norway	0.477	69.563
Vietnam	0.477	10.579
Slovenia	0.479	55.003
Central African Republic	0.480	9.520
Philippines	0.481	11.231
Kazakhstan	0.487	14.438
Madagascar	0.490	9.834
Sudan	0.499	17.698
Mauritania	0.511	14.726
Tanzania	0.514	13.423
Samoa	0.514	16.265
Kenya	0.516	10.632
São Tomé and Príncipe	0.522	13.227
Romania	0.523	26.556
Zambia	0.526	22.972
Guinea	0.532	14.223
Cambodia	0.534	12.629
Estonia	0.537	38.572
Mozambique	0.537	18.714
Guatemala	0.541	17.937

Table A1. Cont.

Country	NTL-Gini	NTL-2020
Sri Lanka	0.547	19.815
Gabon	0.548	17.021
Chad	0.550	23.489
Netherlands	0.550	12.488
Zimbabwe	0.553	34.817
Malawi	0.560	10.926
Somalia	0.577	36.880
Nigeria	0.595	23.318
Afghanistan	0.618	40.357
Uganda	0.624	21.898
Seychelles	0.624	92.991
Lao PDR	0.633	17.154
Namibia	0.636	33.687
Eswatini	0.639	27.596
Burundi	0.642	41.806
Korea, Dem. Rep.	0.642	21.546
Bhutan	0.647	16.960
Eritrea	0.680	72.123
Congo, Dem. Rep.	0.708	64.175
Timor-Leste	0.736	35.984
Cabo Verde	0.746	166.356
St. Kitts and Nevis	0.755	351.285
Papua New Guinea	0.790	651.035
Yemen, Rep.	0.804	562.975
South Sudan	0.831	336.357

References

1. Assembly, G. *Sustainable Development Goals. (SDGs), Transforming Our World: The 2030*; United Nations: New York, NY, USA, 2015.
2. Griggs, D.; Stafford-Smith, M.; Gaffney, O.; Rockström, J.; Öhman, M.C.; Shyamsundar, P.; Steffen, W.; Glaser, G.; Kanie, N.; Noble, I. Policy: Sustainable development goals for people and planet. *Nature* **2013**, *495*, 305. [[CrossRef](#)] [[PubMed](#)]
3. Robert, K.W.; Parris, T.M.; Leiserowitz, A.A. What is sustainable development? Goals, indicators, values, and practice. *Environ. Sci. Policy Sustain. Dev.* **2005**, *47*, 8–21. [[CrossRef](#)]
4. Sachs, J.D. From millennium development goals to sustainable development goals. *Lancet* **2012**, *379*, 2206–2211. [[CrossRef](#)]
5. Andries, A.; Morse, S.; Murphy, R.J.; Lynch, J.; Woolliams, E.R. Seeing Sustainability from Space: Using Earth Observation Data to Populate the UN Sustainable Development Goal Indicators. *Sustainability* **2019**, *11*, 5062. [[CrossRef](#)]
6. Nordhaus, W.; Azam, Q.; Corderi, D.; Hood, K.; Victor, N.M.; Mohammed, M.; Miltner, A.; Weiss, J. *The G-Econ Database on Gridded Output: Methods and Data*; Yale University: New Haven, CT, USA, 2006; Volume 6.
7. Zhang, Q.; Seto, K.C. Mapping urbanization dynamics at regional and global scales using multi-temporal DMSP/OLS nighttime light data. *Remote Sens. Environ.* **2011**, *115*, 2320–2329. [[CrossRef](#)]

8. Baugh, K.; Elvidge, C.D.; Ghosh, T.; Ziskin, D. Development of a 2009 stable lights product using DMSP-OLS data. *Proc. Asia Pac. Adv. Netw.* **2010**, *30*, 114–130. [[CrossRef](#)]
9. Elvidge, C.D.; Baugh, K.E.; Dietz, J.B.; Bland, T.; Sutton, P.C.; Kroehl, H.W. Radiance calibration of DMSP-OLS low-light imaging data of human settlements. *Remote Sens. Environ.* **1999**, *68*, 77–88. [[CrossRef](#)]
10. Doll, C.H.; Muller, J.-P.; Elvidge, C.D. Night-time imagery as a tool for global mapping of socioeconomic parameters and greenhouse gas emissions. *AMBIO J. Hum. Environ.* **2000**, *29*, 157–163. [[CrossRef](#)]
11. Skinner, C. Issues and challenges in census taking. *Annu. Rev. Stat. Appl.* **2018**, *5*, 49–63. [[CrossRef](#)]
12. Elvidge, C.D.; Baugh, K.E.; Anderson, S.J.; Sutton, P.C.; Ghosh, T. The Night Light Development Index (NLDI): A spatially explicit measure of human development from satellite data. *Soc. Geogr.* **2012**, *7*, 23–35. [[CrossRef](#)]
13. Elvidge, C.D.; Sutton, P.C.; Ghosh, T.; Tuttle, B.T.; Baugh, K.E.; Bhaduri, B.; Bright, E. A global poverty map derived from satellite data. *Comput. Geosci.* **2009**, *35*, 1652–1660. [[CrossRef](#)]
14. Ghosh, T.; Anderson, S.J.; Elvidge, C.D.; Sutton, P.C. Using Nighttime Satellite Imagery as a Proxy Measure of Human Well-Being. *Sustainability* **2013**, *5*, 4988–5019. [[CrossRef](#)]
15. Li, X.; Xu, H.; Chen, X.; Li, C. Potential of NPP-VIIRS nighttime light imagery for modeling the regional economy of China. *Remote Sens.* **2013**, *5*, 3057–3081. [[CrossRef](#)]
16. Liu, Z.; He, C.; Zhang, Q.; Huang, Q.; Yang, Y. Extracting the dynamics of urban expansion in China using DMSP-OLS nighttime light data from 1992 to 2008. *Landsc. Urban Plan.* **2012**, *106*, 62–72. [[CrossRef](#)]
17. Welch, R. Monitoring urban population and energy utilization patterns from satellite Data. *Remote Sens. Environ.* **1980**, *9*, 1–9. [[CrossRef](#)]
18. Welch, R.; Zupko, S. Urbanized area energy-utilization patterns from Dmsp data. *Photogramm. Eng. Remote Sens.* **1980**, *46*, 201–207.
19. Huang, Q.; Yang, X.; Gao, B.; Yang, Y.; Zhao, Y. Application of DMSP/OLS nighttime light images: A meta-analysis and a systematic literature review. *Remote Sens.* **2014**, *6*, 6844–6866. [[CrossRef](#)]
20. Elvidge, C.D.; Baugh, K.E.; Zhizhin, M.; Hsu, F.-C. Why VIIRS data are superior to DMSP for mapping nighttime lights. *Proc. Asia Pac. Adv. Netw.* **2013**, *35*, 62–69. [[CrossRef](#)]
21. Hillger, D.; Kopp, T.; Lee, T.; Lindsey, D.; Seaman, C.; Miller, S.; Solbrig, J.; Kidder, S.; Bachmeier, S.; Jasmin, T. First-light imagery from Suomi NPP VIIRS. *Bull. Am. Meteorol. Soc.* **2013**, *94*, 1019–1029. [[CrossRef](#)]
22. Xu, T.; Ma, T.; Zhou, C.; Zhou, Y. Characterizing spatio-temporal dynamics of urbanization in China using time series of DMSP/OLS night light data. *Remote Sens.* **2014**, *6*, 7708–7731. [[CrossRef](#)]
23. Yu, B.; Shi, K.; Hu, Y.; Huang, C.; Chen, Z.; Wu, J. Poverty Evaluation Using NPP-VIIRS Nighttime Light Composite Data at the County Level in China. *IEEE J. Sel. Top. Appl. Earth Obs. Remote Sens.* **2015**, *8*, 1217–1229. [[CrossRef](#)]
24. Hu, T.; Huang, X. A novel locally adaptive method for modeling the spatiotemporal dynamics of global electric power consumption based on DMSP-OLS nighttime stable light data. *Appl. Energy* **2019**, *240*, 778–792. [[CrossRef](#)]
25. Sutton, P.C.; Elvidge, C.D.; Ghosh, T. Estimation of gross domestic product at sub-national scales using nighttime satellite imagery. *Int. J. Ecol. Econ. Stat.* **2007**, *8*, 5–21.
26. Shi, K.; Yu, B.; Huang, Y.; Hu, Y.; Yin, B.; Chen, Z.; Chen, L.; Wu, J. Evaluating the ability of NPP-VIIRS nighttime light data to estimate the gross domestic product and the electric power consumption of China at multiple scales: A comparison with DMSP-OLS data. *Remote Sens.* **2014**, *6*, 1705–1724. [[CrossRef](#)]
27. Bundervoet, T.; Maiyo, L.; Sanghi, A. *Bright Lights, Big Cities: Measuring National and Subnational Economic Growth in Africa from Outer Space, with an Application to Kenya and Rwanda*; The World Bank: Washington, DC, USA, 2015.
28. Townsend, A.C.; Bruce, D.A. The Use of Night-time Lights Satellite Imagery as a Measure of Australia's Regional Electricity Consumption and Population Distribution. *Int. J. Remote Sens.* **2010**, *31*, 4459–4480. [[CrossRef](#)]
29. Birdsall, N. Rising inequality in the new global economy. *Int. J. Dev. Issues* **2006**, *5*, 1–9. [[CrossRef](#)]
30. Liu, F.T.; Ting, K.M.; Zhou, Z.-H. Isolation forest. In Proceedings of the 2008 Eighth IEEE International Conference on Data Mining, Washington, DC, USA, 15–19 December 2008; pp. 413–422.
31. United Nations. *Inequality Measurement*; UN: New York, NY, USA, 2015.
32. Hijmans, R.; Garcia, N.; Wiczorek, J. *Global Administrative Areas Database (GADM) Version 3.6*; UN: New York, NY, USA, 2018.

33. Schiavina, M.; Freire, S.; MacManus, K. GHS population grid multitemporal (1975, 1990, 2000, 2015) R2019A. *Eur. Comm. JRC* **2019**. [[CrossRef](#)]
34. Pesaresi, M.; Florczyk, A.; Schiavina, M.; Melchiorri, M.; Maffenini, L. GHS settlement grid, updated and refined REGIO model 2014 in application to GHS-BUILT R2018A and GHS-POP R2019A, multitemporal (1975-1990-2000-2015), R2019A. *Eur. Comm. JRC* **2019**. Available online: <https://data.europa.eu/euodp/en/data/dataset/42e8be89-54ff-464e-be7b-bf9e64da5218/resource/e8dfcd47-6ff6-4bc1-a1cd-9ffde5405736> (accessed on 1 January 2019).
35. NOAA Version 1 VIIRS Day/Night Band Nighttime Lights. Available online: https://ngdc.noaa.gov/eog/viirs/download_dnb_composites.html (accessed on 01 August 2019).
36. The World Bank. *World Development Indicators*; The World Bank: Washington, DC, USA, 2016.
37. UNDP Income Quintile Ratio. Available online: <http://hdr.undp.org/en/content/income-quintile-ratio> (accessed on 10 May 2019).
38. Elvidge, C.D.; Baugh, K.; Zhizhin, M.; Hsu, F.C.; Ghosh, T. VIIRS night-time lights. *Int. J. Remote Sens.* **2017**, *38*, 5860–5879. [[CrossRef](#)]
39. Wang, R.; Wan, B.; Guo, Q.; Hu, M.; Zhou, S. Mapping regional urban extent using NPP-VIIRS DNB and MODIS NDVI data. *Remote Sens.* **2017**, *9*, 862. [[CrossRef](#)]
40. Ester, M.; Kriegel, H.-P.; Sander, J.; Xu, X. A density-based algorithm for discovering clusters in large spatial databases with noise. *KDD* **1996**, *96*, 226–231.
41. Gini, C. Measurement of inequality of incomes. *Econ. J.* **1921**, *31*, 124–126. [[CrossRef](#)]
42. Gastwirth, J.L. The estimation of the Lorenz curve and Gini index. *Rev. Econ. Stat.* **1972**, *54*, 306–316. [[CrossRef](#)]
43. Kawachi, I.; Kennedy, B.P. The relationship of income inequality to mortality: Does the choice of indicator matter? *Soc. Sci. Med.* **1997**, *45*, 1121–1127. [[CrossRef](#)]
44. Mackenbach, J.P.; Kunst, A.E. Measuring the magnitude of socio-economic inequalities in health: An overview of available measures illustrated with two examples from Europe. *Soc. Sci. Med.* **1997**, *44*, 757–771. [[CrossRef](#)]
45. De Maio, F.G. Income inequality measures. *J. Epidemiol. Community Health* **2007**, *61*, 849–852. [[CrossRef](#)]
46. Sutton, P.C.; Costanza, R. Global estimates of market and non-market values derived from nighttime satellite imagery, land cover, and ecosystem service valuation. *Ecol. Econ.* **2002**, *41*, 509–527. [[CrossRef](#)]
47. Falchetta, G.; Pachauri, S.; Parkinson, S.; Byers, E. A high-resolution gridded dataset to assess electrification in sub-Saharan Africa. *Sci. Data* **2019**, *6*, 110. [[CrossRef](#)]
48. Kumm, M.; Taka, M.; Guillaume, J.H. Gridded global datasets for gross domestic product and Human Development Index over 1990–2015. *Sci. Data* **2018**, *5*, 180004. [[CrossRef](#)]
49. Wackernagel, M.; Onisto, L.; Bello, P.; Linares, A.C.; Falfán, I.S.L.; García, J.M.; Guerrero, A.I.S.; Guerrero, M.G.S. National natural capital accounting with the ecological footprint concept. *Ecol. Econ.* **1999**, *29*, 375–390. [[CrossRef](#)]
50. Costanza, R.; d’Arge, R.; De Groot, R.; Farber, S.; Grasso, M.; Hannon, B.; Limburg, K.; Naeem, S.; O’neill, R.V.; Paruelo, J. The value of the world’s ecosystem services and natural capital. *Nature* **1997**, *387*, 253. [[CrossRef](#)]
51. Imhoff, M.L.; Bounoua, L.; Zhang, P.; Wolfe, R. *Assessing the Urban Heat Island Effect Across Biomes in the Continental USA Using Landsat and MODIS*; NASA: Washington, DC, USA, 2011.

